Mechatronics 25 (2015) 27–36

Contents lists available at ScienceDirect

Mechatronics

journal homepage: www.elsevier.com/locate/mechatronics

Adaptive robust control of fully-constrained cable driven parallel robots

Reza Babaghasabha *, Mohammad A. Khosravi, Hamid D. Taghirad

Advanced Robotics and Automated Systems (ARAS), Industrial Control Center of Excellence (ICCE), Faculty of Electrical Engineering, K.N. Toosi University of Technology, Tehran, Iran

ARTICLE INFO

Article history:
Received 24 June 2014
Accepted 16 November 2014
Available online 11 December 2014

Keywords:
Cable driven parallel robots
Adaptive robust control
Structured and parametric uncertainties
Internal force
Stability analysis
Experimental verification

ABSTRACT

In this paper, adaptive robust control (ARC) of fully-constrained cable driven parallel robots is studied in detail. Since kinematic and dynamic models of the robot are partly structurally unknown in practice, in this paper an adaptive robust sliding mode controller is proposed based on the adaptation of the upper bound of the uncertainties. This approach does not require pre-knowledge of the uncertainties upper bounds and linear regression form of kinematic and dynamic models. Moreover, to ensure that all cables remain in tension, proposed control algorithm benefit the internal force concept in its structure. The proposed controller not only keeps all cables under tension for the whole workspace of the robot, it is chattering-free, computationally simple and it does not require measurement of the end-effector acceleration. The stability of the closed-loop system with proposed control algorithm is analyzed through Lyapunov second method and it is shown that the tracking error will remain uniformly ultimately bounded (UUB). Finally, the effectiveness of the proposed control algorithm is examined through some experiments on a planar cable driven parallel robot and it is shown that the proposed controller is able to provide suitable tracking performance in practice.

© 2014 Elsevier Ltd. All rights reserved.

1. Introduction

Cable driven parallel robots (CDPRs) remedy some shortcomings of the conventional serial and parallel robots. Using cables instead of rigid links in the robot structure has some positive features such as large workspace [1,2], high speed manipulation [3], high payload to robot weight ratio [4], transportability and ease of assembly/disassembly. CDPRs can be classified into two types, namely, fully-constrained and under-constrained robots. In the under-constrained type, a passive force such as gravity is used to keep all the cables under tension. While in the fully-constrained type, the number of actuators are be at least one more than the number of robot degree of freedoms [5]. The cable driven parallel robots which are under study in this paper are restricted to the fully-constrained type and it is assumed that the motion control is performed in the wrench-closure workspace.

Using actuation redundancy in the structure of the parallel robots improves some of kinematic and dynamic properties of parallel robots such as stiffness and singularity avoidance [6,7]. Moreover, actuation redundancy is an important requirement in fully-constrained CDPRs, since cables are able to apply only tensile forces. Hence, the well-known control theories of the parallel robots should be modified such that the cables remain in tension for the whole workspace of CDPRs. For this reason, control of the cable driven parallel robots is more challenging than that of the conventional robots.

Motion control algorithms of CDPRs may be classified based on the coordinates used in the design procedure into two categories, namely the cable length coordinates and the task space coordinates. In the cable length coordinates, decentralized controllers are designed on each of the actuated cables [3,8,9], and the length of the cables which are simply measured by the encoders is used in the feedback structure. However, due to the inherent flexibility of the cables, using cable length in the feedback control loop is not reliable in applications with high accuracy.

In the task space coordinates, the pose of the end-effector is measured directly and it is used as the feedback to the controller [10,11]. Implementation of such measurement is more challenging than that of the cable length measurement. Moreover, it may require expensive instrumentation system such as laser ranging equipment [10,12], or differential GPS (Global Positioning System) augmented by accelerometers and rate gyros [11], or multiple camera with high resolution and high frame rate [13,14]. For this reason, only few researches focus on implementation of the task space controllers in practice, which is considered in this paper in detail.

Motion control algorithms may be classified based on the controller designing technique, as well. Within this classification,

* Corresponding author.
E-mail addresses: Reza.bgha@mail.kntu.ac.ir (R. Babaghasabha), Makh@ee.kntu.ac.ir (M.A. Khosravi), Taghirad@kntu.ac.ir (H.D. Taghirad).

http://dx.doi.org/10.1016/j.mechatronics.2014.11.005
0957-4158/© 2014 Elsevier Ltd. All rights reserved.

classic controllers such as PID [15] are computationally simple and they do not require complete dynamic knowledge of the CDPRs. However, lack of consideration of dynamic effects in the structure of the controller may limit the tracking performance. Nonlinear controllers such as Lyapunov based methods [16,17] and inverse dynamics control (IDC) [18,19] may improve the tracking performance. However, they require complete kinematic and dynamic models of CDPRs with detailed information of the true parameters. It shall be noted that in practice the kinematic and dynamic models of CDPRs possess structured and parametric uncertainties and precise knowledge of the models is unavailable. These issues significantly limit the performance of the nonlinear controllers in tracking objectives. The shortcomings of the parametric uncertainties may be remedied by using an adaptive controller in task space coordinates in which the kinematic and dynamic parameters are simultaneously adapted, which is proposed in this paper.

As a representative of adaptive methods, in [20] robust PD controller with an adaptive compensation term are designed to identify near true kinematic parameters. However, a large number of kinematic parameters has been selected for adaptation and therefore, the controller is computationally expensive. In order to improve performance of such adaptive methods, in [21,22] two adaptive control scheme is proposed by considering uncertainties in dynamic and kinematic parameters. However, these approaches require the linear regression form of kinematic and dynamic models. Moreover, structured uncertainties of the kinematic and dynamic models and external disturbances, directly affect the updated parameters and degrade the performance of the controller.

In order to reduce the effect of both structured and parametric uncertainties, in [23] sliding mode controller is designed based on knowledge of the uncertainties upper bound of the kinematic and dynamic models. However, from a practical point of view, determination of the uncertainties upper bound is a prohibitive task, and therefore, it is often over-estimated which yields to excessive controller gains. This fact amplify the main drawback of the sliding mode control, namely the chattering phenomenon, and significantly degrade the performance of the controller.

The goal of this paper is to design a controller to improve the performance of the fully-constrained cable driven parallel robots in presence of structured and parametric uncertainties. To develop the idea, an adaptive robust sliding mode controller is designed based on the adaptation of the uncertainties upper bound. It is assumed that all terms in the dynamic and kinematic model of the robot are uncertain and the precise pre-knowledge about their upper bounds is also unavailable in practice. The proposed controller will significantly remove the effect of excessive gain and it is chattering-free. Moreover, this approach does not require the linear regression form of kinematic and dynamic models. In addition, the internal force concept is used in the proposed controller to provide positive tension of the cables. The stability of the closed-loop system with proposed control algorithm is analyzed through Lyapunov second method. Finally, the effectiveness of the proposed controller is examined through some experiments on a planar cable driven parallel robot with four actuated cable-driven limbs and it is shown that the proposed controller is able to provide suitable tracking performance in practice.

The paper is organized as follows. In Section 2 some important properties of kinematic and dynamic models of the CDPRs are denoted. Section 3 focuses on the controller design in which the proposed adaptive robust controller is introduced and the adaptation law is defined based on the adaptation of the uncertainties upper bound. Then, stability of the closed loop system is analyzed through Lyapunov second method. Finally, in Section 4 experimental results on a planar CDPR is discussed in detail.

2. Robot kinematics and dynamics

Cable driven parallel robot has a closed kinematic chain mechanism in which a number of actuated cables provide connection between the base and the end-effector. Furthermore, the electrical actuators lead the end-effector toward a desired pose by changing the length of the cables. In [15] kinematic and dynamic analysis of fully-constrained CDPRs have been reported in detail. In this paper, we leave the details of the formulation and only denote some important properties of kinematic and dynamic formulations, which are used in the controller design. The dynamic model of a fully-constrained CDPR without considering the flexibility of the cables may be written as:

$$\boldsymbol{M}(\boldsymbol{x})\ddot{\boldsymbol{x}} + \boldsymbol{C}(\boldsymbol{x},\dot{\boldsymbol{x}})\dot{\boldsymbol{x}} + \boldsymbol{G}(\boldsymbol{x}) + \boldsymbol{N}(\dot{\boldsymbol{x}}) + \boldsymbol{T}_d = -\boldsymbol{J}^T\boldsymbol{\tau} \tag{1}$$

in which,

$$\boldsymbol{N}(\dot{\boldsymbol{x}}) = \boldsymbol{F}_d\dot{\boldsymbol{x}} + \boldsymbol{F}_s(\dot{\boldsymbol{x}})$$

where $\boldsymbol{x}$ denotes the generalized coordinates vector for pose of the end-effector, $\boldsymbol{M}(\boldsymbol{x})$ is mass matrix of the robot, $\boldsymbol{C}(\boldsymbol{x},\dot{\boldsymbol{x}})$ denotes Coriolis and centrifugal terms and $\boldsymbol{G}(\boldsymbol{x})$ indicates the vector of gravity terms, $\boldsymbol{F}$ denotes the vector of Cartesian wrench, $\boldsymbol{\tau}$ is the vector of cable forces and $\boldsymbol{J}$ denotes the Jacobian matrix of the robot. Furthermore, $\boldsymbol{F}_d$ denotes the coefficient matrix of viscous friction, $\boldsymbol{F}_s$ is the Coulomb friction term and $\boldsymbol{T}_d$ denotes disturbance which may represent any inaccuracy in dynamic model. Although the dynamic model described by (1) is nonlinear and multi-input/multi-output (MIMO), it has some useful properties that are listed as follows [15]:

Property 1. *The mass matrix $\boldsymbol{M}(\boldsymbol{x})$ is symmetric, uniformly positive definite and bounded from above and below for all $\boldsymbol{x}$ by:*

$$\underline{m} \leqslant \|\boldsymbol{M}(\boldsymbol{x})\| \leqslant \overline{m} \tag{2}$$

Property 2. *Upper bound of the Coriolis and centrifugal matrix is independent of $\boldsymbol{x}$, and is a function of only $\dot{\boldsymbol{x}}$ as:*

$$\|\boldsymbol{C}(\boldsymbol{x},\dot{\boldsymbol{x}})\| \leqslant \xi_c\|\dot{\boldsymbol{x}}\| \tag{3}$$

Property 3. *The matrix $\dot{\boldsymbol{M}}(\boldsymbol{x}) - 2\boldsymbol{C}(\boldsymbol{x},\dot{\boldsymbol{x}})$ is skew-symmetric and therefore, for all $\boldsymbol{Z}$:*

$$\boldsymbol{Z}^T(\dot{\boldsymbol{M}}(\boldsymbol{x}) - 2\boldsymbol{C}(\boldsymbol{x},\dot{\boldsymbol{x}}))\boldsymbol{Z} = 0 \tag{4}$$

Property 4. *Coulomb and viscous friction terms are dissipative and they have an upper bound as:*

$$\|\boldsymbol{F}_d\dot{\boldsymbol{x}} + \boldsymbol{F}_s(\dot{\boldsymbol{x}})\| \leqslant \xi_{f_0}\|\dot{\boldsymbol{x}}\| + \xi_{f_1} \tag{5}$$

Property 5. *Gravity vector and disturbance term have upper bounds of:*

$$\|\boldsymbol{G}(\boldsymbol{x})\| \leqslant \xi_g, \qquad \|\boldsymbol{T}_d\| \leqslant \xi_t \tag{6}$$

3. Adaptive robust control of cable robots

In this section, considering the structured and parametric uncertainties in kinematic and dynamic models of the robot, an adaptive robust control algorithm is proposed. This control algorithm consists of an adaptive robust sliding mode control whose adaptation law is only based on the adaptation of only the uncertainties upper bound. To derive the control and adaptation laws, consider the following Lyapunov function candidate as:

$$V(t) = \frac{1}{2}(\boldsymbol{S}^T\boldsymbol{M}\boldsymbol{S} + \tilde{\boldsymbol{\rho}}^T\boldsymbol{\Gamma}\tilde{\boldsymbol{\rho}}) \tag{7}$$

in which,

$$\boldsymbol{S} = \dot{\tilde{\boldsymbol{x}}} + \boldsymbol{\Lambda}\tilde{\boldsymbol{x}} \tag{8}$$

where, $\boldsymbol{S} = [S_1, \ldots, S_n]^T$ is a sliding surface vector, $\boldsymbol{\Gamma} = \text{diag}(\Gamma_1, \ldots, \Gamma_n)$ and $\boldsymbol{\Lambda} = \text{diag}(\Lambda_1, \ldots, \Lambda_n)$ are symmetric diagonal positive definite matrices, n denotes the degrees of freedom of the robot, $\tilde{\boldsymbol{x}} = \boldsymbol{x} - \boldsymbol{x}_d$ is the tracking error vector and $\tilde{\boldsymbol{\rho}} = \hat{\boldsymbol{\rho}} - \boldsymbol{\rho}$ denotes the uncertainties upper bound estimation error vector. Differentiate $V(t)$ with respect to time:

$$\begin{aligned}\dot{V}(t) &= \boldsymbol{S}^T\boldsymbol{M}\dot{\boldsymbol{S}} + \frac{1}{2}\boldsymbol{S}^T\dot{\boldsymbol{M}}\boldsymbol{S} + \tilde{\boldsymbol{\rho}}^T\boldsymbol{\Gamma}\dot{\tilde{\boldsymbol{\rho}}} \\ &= \boldsymbol{S}^T\boldsymbol{M}(\ddot{\tilde{\boldsymbol{x}}} + \boldsymbol{\Lambda}\dot{\tilde{\boldsymbol{x}}}) + \boldsymbol{S}^T\left[\frac{1}{2}(\dot{\boldsymbol{M}} - 2\boldsymbol{C}) + \boldsymbol{C}\right]\boldsymbol{S} + \tilde{\boldsymbol{\rho}}^T\boldsymbol{\Gamma}\dot{\tilde{\boldsymbol{\rho}}}\end{aligned} \tag{9}$$

Using skew-symmetricity property of $\dot{\boldsymbol{M}} - 2\boldsymbol{C}$ and substitution from (1) yields to:

$$\dot{V}(t) = \boldsymbol{S}^T[-\boldsymbol{J}^T\boldsymbol{\tau} - (\boldsymbol{C}\dot{\boldsymbol{x}} + \boldsymbol{G} + \boldsymbol{N} + \boldsymbol{T}_d) - \boldsymbol{M}\ddot{\boldsymbol{x}}_d + \boldsymbol{M}\boldsymbol{\Lambda}\dot{\tilde{\boldsymbol{x}}} + \boldsymbol{C}\boldsymbol{S}] + \tilde{\boldsymbol{\rho}}^T\boldsymbol{\Gamma}\dot{\tilde{\boldsymbol{\rho}}} \tag{10}$$

Define the virtual reference trajectory as

$$\boldsymbol{x}_r = \boldsymbol{x}_d - \boldsymbol{\Lambda}\int_0^t \tilde{\boldsymbol{x}}dt \tag{11}$$

Differentiate $\boldsymbol{x}_r$ twice with respect to time, and substitute into Eq. (10) yields to:

$$\dot{V}(t) = \boldsymbol{S}^T[-\boldsymbol{J}^T\boldsymbol{\tau} - (\boldsymbol{M}\ddot{\boldsymbol{x}}_r + \boldsymbol{C}\dot{\boldsymbol{x}}_r + \boldsymbol{G} + \boldsymbol{N} + \boldsymbol{T}_d)] + \tilde{\boldsymbol{\rho}}^T\boldsymbol{\Gamma}\dot{\tilde{\boldsymbol{\rho}}} \tag{12}$$

Let us define the control law as

$$\boldsymbol{F} = -\widehat{\boldsymbol{J}}^T\boldsymbol{\tau} = \widehat{\boldsymbol{M}}\ddot{\boldsymbol{x}}_r + \widehat{\boldsymbol{C}}\dot{\boldsymbol{x}}_r + \widehat{\boldsymbol{G}} + \widehat{\boldsymbol{N}} - \boldsymbol{K}_D\,\text{sgn}(\boldsymbol{S}) \tag{13}$$

in which,

$$\text{sgn}\ (S_i) = \begin{cases} 1 & S_i > 0 \\ 0 & S_i = 0 \\ -1 & S_i < 0 \end{cases}$$

where $\widehat{\boldsymbol{M}}, \widehat{\boldsymbol{C}}, \widehat{\boldsymbol{G}}, \widehat{\boldsymbol{N}}$ are available estimations of dynamic terms, $\boldsymbol{K}_D = \text{diag}(k_{d_1}, \ldots, k_{d_n})$ is symmetric diagonal positive definite matrix and $\widehat{\boldsymbol{J}}^T$ denotes estimated Jacobian matrix of the robot. It is assumed that the attachment points are not precisely mounted in practice. Therefore, Jacobian matrix of the robot is uncertain due to the uncertainty in some of the kinematic parameters. The general solution of (13) for $\boldsymbol{\tau}$ is

$$\boldsymbol{\tau} = \overline{\boldsymbol{\tau}} + \boldsymbol{Q} \tag{14}$$

where $\overline{\boldsymbol{\tau}}$ is the minimum norm solution of (13) which is derived by using the pseudo-inverse of $\widehat{\boldsymbol{J}}^T$ as:

$$\overline{\boldsymbol{\tau}} = -\widehat{\boldsymbol{J}}(\widehat{\boldsymbol{J}}^T\widehat{\boldsymbol{J}})^{-1}\boldsymbol{F} = -\widehat{\boldsymbol{J}}^{\dagger}\boldsymbol{F} \tag{15}$$

The term $\boldsymbol{Q}$ may be physically interpreted as the internal forces that spans the null space of $\widehat{\boldsymbol{J}}^T$, by which

$$\widehat{\boldsymbol{J}}^T\boldsymbol{Q} = 0 \tag{16}$$

Internal forces are used to keep all cables under tension within the whole workspace of the robot. Moreover, this term may be used to increase the robot stiffness [24]. Now, substitute the control law (14) into Eq. (12). This yields to:

$$\begin{aligned}\dot{V}(t) &= \boldsymbol{S}^T[(\boldsymbol{J}^T\widehat{\boldsymbol{J}}^{\dagger})\boldsymbol{F} - \boldsymbol{J}^T\boldsymbol{Q} - (\boldsymbol{M}\ddot{\boldsymbol{x}}_r + \boldsymbol{C}\dot{\boldsymbol{x}}_r + \boldsymbol{G} + \boldsymbol{N} + \boldsymbol{T}_d)] + \tilde{\boldsymbol{\rho}}^T\boldsymbol{\Gamma}\dot{\tilde{\boldsymbol{\rho}}} \\ &= \boldsymbol{S}^T[(\boldsymbol{J}^T\widehat{\boldsymbol{J}}^{\dagger})\boldsymbol{F} + \boldsymbol{F} - \boldsymbol{F} - \boldsymbol{J}^T\boldsymbol{Q} + \widehat{\boldsymbol{J}}^T\boldsymbol{Q} - (\boldsymbol{M}\ddot{\boldsymbol{x}}_r + \boldsymbol{C}\dot{\boldsymbol{x}}_r + \boldsymbol{G} + \boldsymbol{N} \\ &\quad + \boldsymbol{T}_d)] + \tilde{\boldsymbol{\rho}}^T\boldsymbol{\Gamma}\dot{\tilde{\boldsymbol{\rho}}} \\ &= \boldsymbol{S}^T[-\boldsymbol{K}_D\,\text{sgn}(\boldsymbol{S}) - (\boldsymbol{I} - \boldsymbol{J}^T\widehat{\boldsymbol{J}}^{\dagger})\boldsymbol{F} - (\boldsymbol{J}^T - \widehat{\boldsymbol{J}}^T)\boldsymbol{Q} + (\widetilde{\boldsymbol{M}}\ddot{\boldsymbol{x}}_r \\ &\quad + \widetilde{\boldsymbol{C}}\dot{\boldsymbol{x}}_r + \widetilde{\boldsymbol{G}} + \widetilde{\boldsymbol{N}}) - \boldsymbol{T}_d] + \tilde{\boldsymbol{\rho}}^T\boldsymbol{\Gamma}\dot{\tilde{\boldsymbol{\rho}}}\end{aligned} \tag{17}$$

in which,

$$\widetilde{\boldsymbol{M}} = \widehat{\boldsymbol{M}} - \boldsymbol{M}, \quad \widetilde{\boldsymbol{C}} = \widehat{\boldsymbol{C}} - \boldsymbol{C}, \quad \widetilde{\boldsymbol{G}} = \widehat{\boldsymbol{G}} - \boldsymbol{G}, \quad \widetilde{\boldsymbol{N}} = \widehat{\boldsymbol{N}} - \boldsymbol{N}$$

The uncertain Jacobian matrix $\widehat{\boldsymbol{J}}^T$, and the internal forces may be assumed to be bounded by the following relations:

$$\|(\boldsymbol{J}^T - \widehat{\boldsymbol{J}}^T)\boldsymbol{Q}\| \leqslant \xi_Q \tag{18}$$

$$\|(\boldsymbol{I} - \boldsymbol{J}^T\widehat{\boldsymbol{J}}^{\dagger})\boldsymbol{F}\| \leqslant \xi_J\|\boldsymbol{S}\| \tag{19}$$

According to the above inequalities and the properties of the robot dynamic model, which are denoted in Section 2, it may be concluded that:

$$\begin{aligned}&\|(\widetilde{\boldsymbol{M}}\ddot{\boldsymbol{x}}_r + \widetilde{\boldsymbol{C}}\dot{\boldsymbol{x}}_r + \widetilde{\boldsymbol{G}} + \widetilde{\boldsymbol{N}}) - \boldsymbol{T}_d - (\boldsymbol{I} - \boldsymbol{J}^T\widehat{\boldsymbol{J}}^{\dagger})\boldsymbol{F} - (\boldsymbol{J}^T - \widehat{\boldsymbol{J}}^T)\boldsymbol{Q}\| \\ &\quad \leqslant \sum_{i=1}^{n}\rho_i(S_i, t)\end{aligned} \tag{20}$$

Using this inequality one may rewrite $\dot{V}(t)$ as

$$\dot{V}(t) \leqslant \sum_{i=1}^{n}|S_i|[-k_{d_i} + \rho_i] + \tilde{\rho}_i\Gamma_i\dot{\tilde{\rho}}_i \tag{21}$$

Now, assume that:

$$k_{d_i} = k_i + \hat{\rho}_i \tag{22}$$

in which, k_i is a positive parameter, and substitute it into Eq. (21):

$$\dot{V}(t) \leqslant \sum_{i=1}^{n}|S_i|[-k_i - \tilde{\rho}_i] + \tilde{\rho}_i\Gamma_i\dot{\tilde{\rho}}_i \tag{23}$$

Let us propose the following adaptation law:

$$\dot{\tilde{\rho}}_i = \dot{\hat{\rho}}_i = \Gamma_i^{-1}|S_i| \tag{24}$$

By using the above adaptation law, the resulting expression of $\dot{V}(t)$ is reduced to:

$$\dot{V}(t) \leqslant \sum_{i=1}^{n} - k_i|S_i| \leqslant 0 \tag{25}$$

which is negative semi-definite. This result shows that the proposed controller can stabilize the system and the trajectories of the closed loop system will eventually converges to the sliding surface,

$$\boldsymbol{S} = \dot{\tilde{\boldsymbol{x}}} + \boldsymbol{\Lambda}\tilde{\boldsymbol{x}} = 0 \tag{26}$$

Therefore, the proposed adaptive controller guarantees zero steady-state tracking error. The main feature of this approach is that the result is not in debt of finding a linear regression form for kinematic and dynamic models, and furthermore, it does not require a priori knowledge on the uncertainties upper bound.

As it can be seen in adaptation law (24), the value of $\dot{\hat{\rho}}_i$ is zero only when the value of S_i is zero, otherwise the value of $\hat{\rho}_i$ always increases. However, in practice, steady-state tracking error cannot remain on sliding surface due to the measurement noise. In this case, the control gain k_{d_i} is clearly over-estimated with respect to uncertainties, which induces chattering. In order to avoid increasing the control gains, it is proposed to modify the control law (13) and the adaptation law (24) as following:

$$\boldsymbol{F} = -\widehat{\boldsymbol{J}}^T\boldsymbol{\tau} = \widehat{\boldsymbol{M}}\ddot{\boldsymbol{x}}_r + \widehat{\boldsymbol{C}}\dot{\boldsymbol{x}}_r + \widehat{\boldsymbol{G}} + \widehat{\boldsymbol{N}} - \boldsymbol{K}_D\tanh\left(\frac{\boldsymbol{S}}{\boldsymbol{\epsilon}}\right) \tag{27}$$

and

$$\dot{\hat{\rho}}_i = \Gamma_i^{-1}|S_i|\,\text{sgn}((|S_i| - \epsilon_i)\hat{\rho}_i) \tag{28}$$

where $\boldsymbol{\epsilon} = \text{diag}(\epsilon_1, \ldots, \epsilon_n)$ is a threshold width on the $\boldsymbol{S}$ variable and it is chosen based on the measurement noise amplitude. This modification of control and adaptation law will significantly removes the effect of excessive gain and generates a chattering free

output. This modification will induce the controller gains as follows:

- If $|S_i| \geqslant \epsilon_i$, then the sign of adaptation law (28) is positive and the gain k_{d_i} is increasing up to a large enough value to counteract the bounded uncertainty, and as a result, the tracking error approaches the sliding surface.
- As long as the trajectories reaches within the boundary layer in which, the $|S_i| < \epsilon_i$, then the sign of adaptation law (28) becomes negative and the gain k_{d_i} reduces to a value which is proportional to the current uncertainties. With this adaptation law, the minimum value of k_{d_i} is set to k_i.
- Now, if an additional load or an external disturbance is applied to the robot and it makes $|S_i| \geqslant \epsilon_i$, according to above algorithm, the control gain k_{d_i} is adjusted with respect to the current uncertainties.

Although such modification improve the performance of the proposed controller in practice, the stability analysis performed on the closed loop system is not valid any more, and this change in the control and adaptation law may affect the asymptotic tracking performance. In order to analyze stability of the closed loop system, consider the same Lyapunov function given in (7), take the derivative with respect to time and substitute the modified control law (27) and the modified adaptation law (28). For $|S_i| \geqslant \epsilon_i$, the same stability analysis for the closed loop system holds and the trajectory tracking eventually converges to the boundary of sliding surface. However, as long as the trajectory reaches within the boundary layer, and $|S_i| < \epsilon_i$, then the derivative of the Lyapunov function with respect to time, given in (21) changes to:

$$\dot{V}(t) \leqslant \sum_{i=1}^{n} |S_i| \left[-k_{d_i} \left(\frac{|S_i|}{\epsilon_i} \right) + \rho_i \right] + \tilde{\rho}_i \Gamma_i \dot{\tilde{\rho}}_i \tag{29}$$

Use the modified adaptation law (28) and simplify as follows:

$$\begin{aligned} \dot{V}(t) &\leqslant \sum_{i=1}^{n} |S_i| \left[-k_{d_i} \left(\frac{|S_i|}{\epsilon_i} \right) + (\rho_i - \tilde{\rho}_i) \right] \\ &\leqslant \sum_{i=1}^{n} |S_i| \left[-k_{d_i} \left(\frac{|S_i|}{\epsilon_i} \right) + (2\rho_i - \hat{\rho}_i) \right] \\ &\leqslant \sum_{i=1}^{n} |S_i| \left[-k_i \left(\frac{|S_i|}{\epsilon_i} \right) + 2\rho_i \right] \end{aligned} \tag{30}$$

In this case, $\dot{V}(t)$ is negative semi-definite only if

$$|S_i| > \left(\frac{2\rho_i}{k_i} \right) \epsilon_i = \delta_{s_i} \tag{31}$$

Therefore, the proposed controller can stabilize the system and the tracking error will remain uniformly ultimately bounded (UUB). However, as it is seen in Eq. (31), the radius of ultimate steady state tracking error δ_{s_i} is dependent on the uncertainties upper bound ρ_i, the parameter k_i and the threshold ϵ_i. This implies that in order to decrease the steady state tracking error, we may increase the gain k_i and therefore, increase the required control effort.

4. Experimental results

In order to verify the effectiveness of the proposed adaptive robust controller, it is applied to KNTU planar cable driven parallel robot. This manipulator is under investigation for high speed and wide workspace applications in Advanced Robotics and Automated Systems (ARAS) group of K.N. Toosi University of Technology.

4.1. Experimental setup

KNTU planar cable driven robot consists of four actuated cable-driven limbs with three degrees of freedom planar motion which is shown in Fig. 1. Actuators are located on the vertices of a rectangle with dimension of 2.24 m × 2.1 m to provide a relatively large

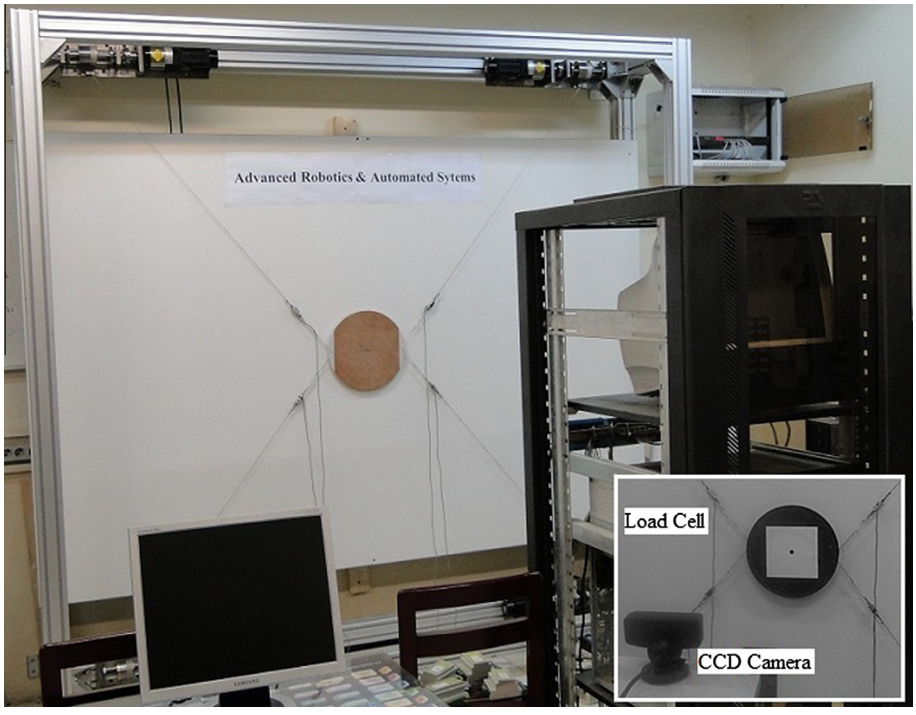

Fig. 1. KNTU planar cable-driven parallel robot.

workspace. Inertial parameters of the planar cable robot is given in Table 1. Moreover, the actual tensions of the cables are measured by the load cells located near the end-effector attachment points. TLL500 product from Transducer Techniques is used as suitable load cell in the experiments due to their relatively large measurement range and low weight.

The block diagram of control system setup is shown in Fig. 2. The host computer serves as the user interface and enables the user to edit and modify control structure and parameters. The target computer is a real time processing unit in which QNX operating system is used and performs real time execution of the control algorithm and real time communication with I/Os. RT-LAB software is used with Simulink to define models in real time environment. RT-LAB is designed to automate the execution of control law for the controllers built in Simulink, in a real time multiprocessing environment [25]. A number of Advantech PCI input/output boards were integrated with the RT-LAB and Simulink to create a real time control system which the sampling time of the control loop is one millisecond.

In addition, a CCD camera with a resolution of 320 × 240 pixels and frame rate of 100 fps at the distance of 1.12 m from the plane of motion of the end-effector is used to directly measure the pose of the end-effector [26]. A square marker is used for fast and accurate tracking and the pose of the end-effector is measured by extracting corners using Harris corner detector [27]. By this means, the resolution of the position and orientation measurement of the end-effector are 0.1 mm and 0.2 degree, respectively. In order to synchronize the sampling time of the control loop and the vision system, the measured pose of the end-effector is repeated during 0.01 s. This result in the sampling time of the entire control loop to be one millisecond despite the lower frame per second capacity of the camera, which is suitable for real time execution of the proposed controller.

Table 1
Inertial parameters of the planar cable robot.

Parameter	Symbol	Value
End-effector mass	m	2.5 kg
End-effector inertia	I_z	0.1 kg m^2
Gear ratio	N	50
Gravity Acceleration	g	9.8 m/s^2
Drum radius	r	3.5 cm

4.2. Dynamic model of KNTU cable robot

According to dynamic model described by (1) and since the motion of KNTU cable robot is planar, we have $\boldsymbol{C}(\boldsymbol{x},\dot{\boldsymbol{x}}) = \boldsymbol{0}$. In this case, the equations of motion for robot can be written as:

$$\boldsymbol{M}(\boldsymbol{x})\ddot{\boldsymbol{x}} + \boldsymbol{G}(\boldsymbol{x}) + \boldsymbol{N}(\dot{\boldsymbol{x}}) + \boldsymbol{T}_d = -\boldsymbol{J}^T\boldsymbol{\tau} \tag{32}$$

where

$$\boldsymbol{N}(\dot{\boldsymbol{x}}) = \boldsymbol{F}_d\dot{\boldsymbol{x}} + \boldsymbol{F}_s(\dot{\boldsymbol{x}})$$

in which

$$\boldsymbol{M} = \begin{bmatrix} m & 0 & 0 \\ 0 & m & 0 \\ 0 & 0 & I_z \end{bmatrix}, \quad \boldsymbol{G} = \begin{bmatrix} 0 \\ mg \\ 0 \end{bmatrix}$$

4.3. Control scheme

According to (14), positive tension of the cables is the output of the proposed control algorithm. These tension of the cables should be accurately provided by the servo drives of the electrical actuators in order to have a desirable performance in tracking the desired trajectories. However, in practice, the actuator drivers suffer from a number of limitations, and cannot perform as ideal torque sources. Moreover, in the design of the proposed controller, it is assumed that the cables are rigid. However, in practice, the cables are flexible element and the actual tensions can never track the desired tensions perfectly. In order to overcome these shortcomings, cascade control scheme, as it is shown in Fig. 3, is implemented on the system. The main purpose of using cascade scheme in control structure of the robot is to obtain a desirable bandwidth for the inner loop which is much larger than that for the outer control loop, and hence, to provide a near ideal torque source for the outer loop.

In this scheme, proposed adaptive robust controller controls the pose of the end-effector in the outer loop. Inputs of the proposed controller are pose errors and the uncertainties upper bound estimation vector, while its outputs are the required Cartesian wrench according to (27). The calculated output wrench is transformed into positive tension of the cables through the internal force control block according to (14). Next, the resulting desired positive tensions are compared to the actual tensions measured by the load

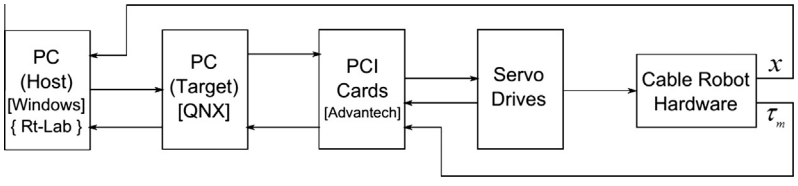

Fig. 2. Control system setup.

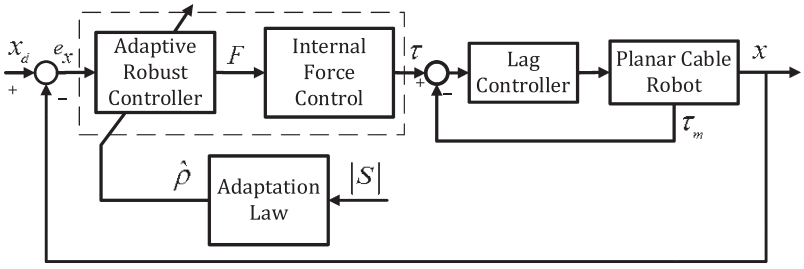

Fig. 3. Block diagram of the proposed adaptive robust controller.

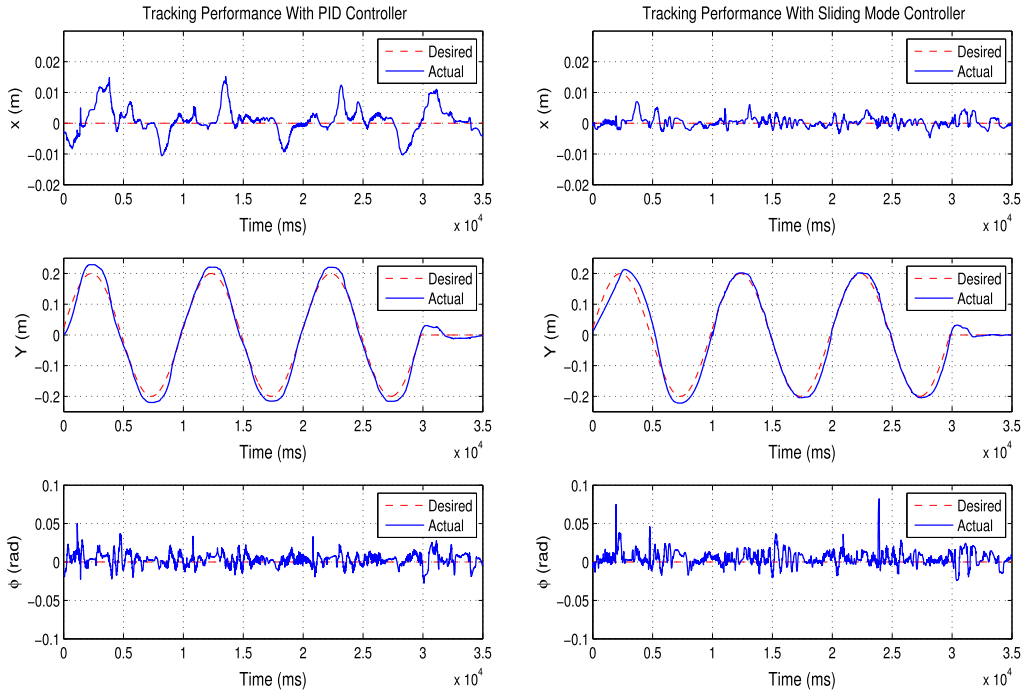

(a) A well tuned PID controller

(b) Sliding mode controller

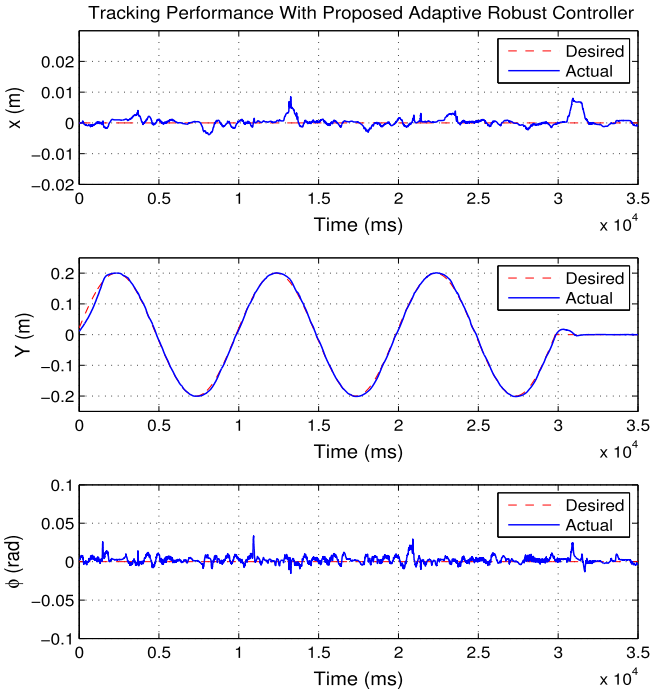

(c) Proposed controller

Fig. 4. Tracking performance of the first desired trajectory.

cells. Finally, four lag controllers are designed in the inner loop on each of the cables to produce a control action according to the tension error. The main goal of these controllers is to filter the high frequency control actions, regulates the cables tension, and prevents them from tearing. Stability of the overall system can be ensured provided that the equivalent bandwidth of the inner loop is larger than the equivalent bandwidth of the outer loop [28].

4.4. Results

In order to verify the effectiveness of the proposed controller, two sets of experiment are performed on KNTU planar cable driven robot and the results of the proposed adaptive robust controller (ARC) are compared with that of a PID controller and a pure sliding mode controller (SMC). In the first set of experiment, a trajectory in Y direction is considered under gravity force, and it is supposed

that the end-effector does not move in the other directions. Note that X direction is horizontal and Y direction is vertical relative to the robot configuration. Moreover, a more challenging circular trajectory with a radius of 0.2 m is considered in the second experiment. Circular trajectory is more challenging than the disjointed trajectory, since in this type of motion the desired trajectories in X and Y directions are considered while zero rotational motion is demanded during the robot movements. In addition, repeatability test is performed in the tracking the circular trajectory for more than one turn. These set of experiments aimed to evaluate the performance of the proposed controller under structured and parametric uncertainties of the robot. It is assumed that the precise knowledge of the mass and the moment of inertia of the end-effector, the kinematic parameters and the inertia and friction parameters of the actuators are unavailable in practice.

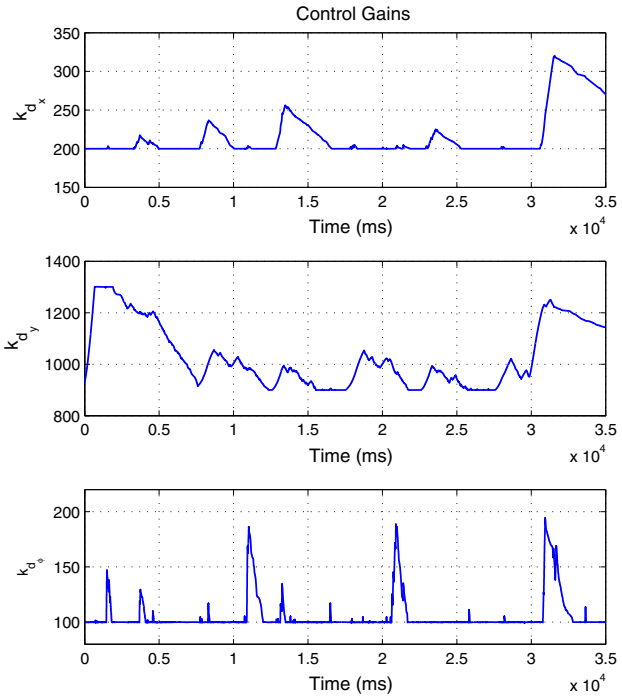

Fig. 5. Adaptation of the control gains in three directions for the first experiment.

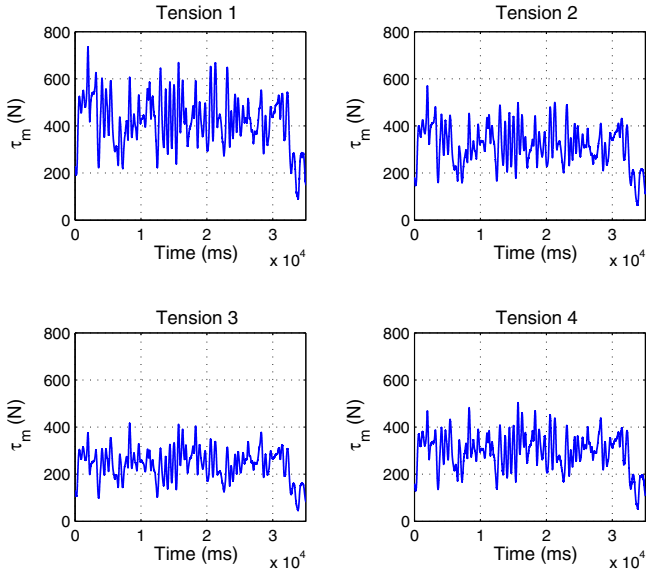

Fig. 6. Cables forces in the first experiment.

In the first experiment, the following sinusoidal trajectory is considered in Y direction while the end-effector attempts to maintain zero translation in X direction and zero rotation in ϕ.

$$y_d = 0.2\sin(0.2\pi t)$$

Fig. 4(a) shows the results of implementation of PID controller in tracking the desired trajectories in three directions. Note that in these figures desired trajectories are drawn in dashed line, while the actual results of implementation are drawn in solid line. As it is seen in this figure, while the controller gains are tuned in an exhaustive procedure, the PID controller cannot suitably track the desired trajectories due to the lack of consideration of dynamic effects in the structure of the controller. In this case, the variable coulomb friction of the actuators has the most significant dynamic effect, and as it can be seen in this figure, it causes large errors where direction of the desired trajectories is changing. Fig. 4(b) shows tracking of the desired trajectories using sliding mode controller. Although the performance of the sliding mode controller in term of compensating the dynamic effects of the robot is much better than that of the PID controller, however relatively long initial time is needed to reach the sliding surface due to the lack of adaptation of the control gains. Fig. 4(c) verifies the effectiveness of the proposed adaptive robust controller in terms of tracking of the desired trajectories. In the proposed controller, by adaptation of the control gains with respect to uncertainties, counteracts the structured and parametric uncertainties and provides suitable tracking performance with suitable accuracy. Fig. 5 shows the adaptation of control gains in three directions. As it is shown in this figure, when the tracking errors slip away from the sliding surface, the control gains is increasing up to a value large enough to counteract the bounded uncertainties. As the trajectories approach the sliding surface, the control gains decreases, in order to use minimum tension in the cables. Since the attachment points of the cables on the end-effector cannot experience any tensions greater than 1000 Newtons, the tension of the cables is limited in practice, by considering an upper bound for the control gains. Moreover, it is observed in Fig. 6 that all cables remain in tension during the robot maneuvers. Finally, from the experimental results, the prescribed uniformly ultimately bounded tracking error for the control structure is verified in all three directions in this experiment.

In the second experiment, the following circular trajectory with a radius of 0.2 meter is considered while the end-effector attempting to maintain $\phi = 0$ at all time.

$$\begin{cases} x_d = 0.2\cos(0.2\pi t)u_s(t-2.5) \\ y_d = 0.2\sin(0.2\pi t)u_s(t) \end{cases}$$

where, $u_s(t)$ denotes unit step function. Fig. 7(a) and 8(a) represent the results of implementation using PID controller. As it is observed in Fig. 7(a), the PID controller has not the desirable performance in tracking the circular trajectory. Moreover, Fig. 8(a) shows that the controller cannot accurately maintain the orientation of the end-effector at zero level. In this case, maximum value of rotation error is 0.07 radian which is relatively large. Fig. 7(b) and 8(b) show tracking of the circular trajectory with sliding mode controller. As mentioned earlier, sliding mode controller has no suitable performance in reaching phase to the sliding surface, which is clearly seen at the left half of circular path in Fig. 7(b). Moreover, the maximum of rotation error is 0.05 radian which is relatively similar to that of the PID controller. Fig. 7(c) verifies the suitable performance of the proposed adaptive robust controller in terms of tracking of the circular trajectory in XY plane. Furthermore, the proposed controller with adaptation of the control gains is successful to decrease the

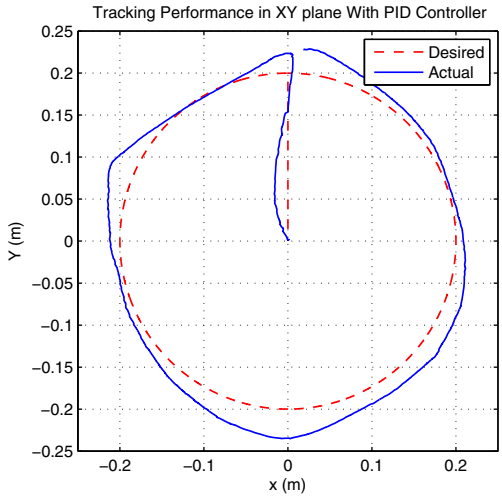

(a) A well tuned PID controller

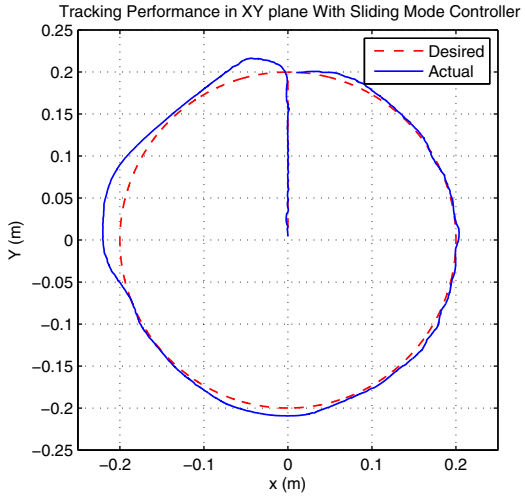

(b) Sliding mode controller

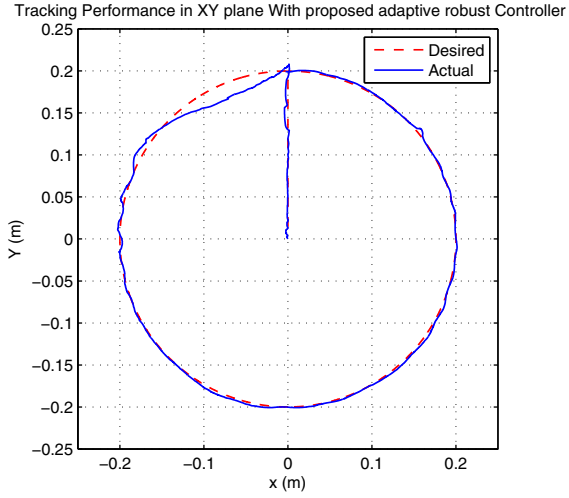

(c) Proposed controller

Fig. 7. Tracking performance of a desired circular trajectory.

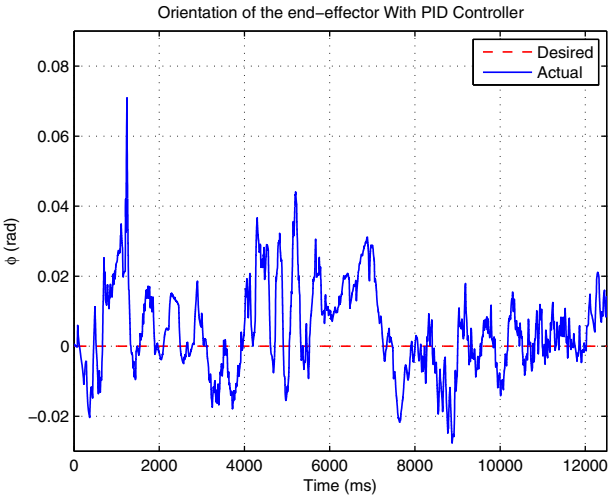

(a) A well tuned PID controller

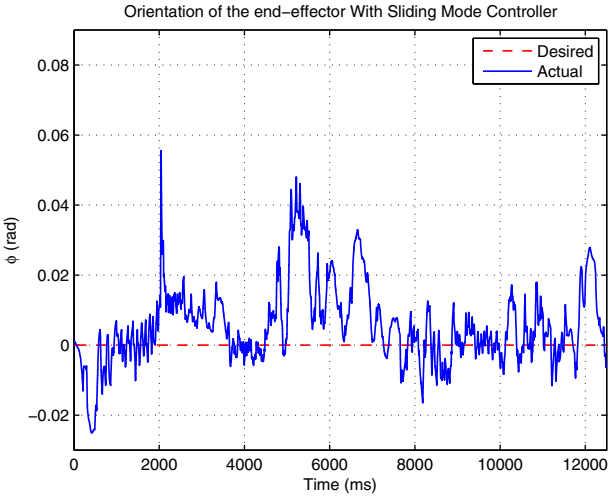

(b) Sliding mode controller

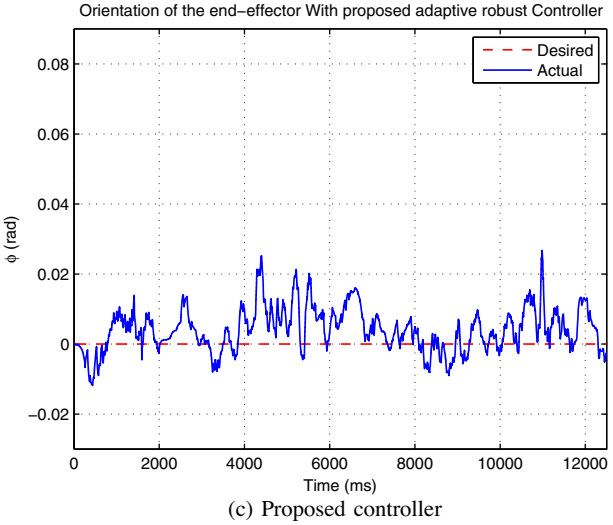

(c) Proposed controller

Fig. 8. Orientation of the end-effector in the second experiment.

time required for reaching phase. In addition, as it is shown in Fig. 8(c), the maximum value of rotation error is 0.02 radian which is almost three times smaller than that of the other two methods. Finally, Fig. 9 shows that the proposed controller keeps all the cables under tension during whole robot maneuver. It may be concluded that the tracking performance of the proposed adaptive

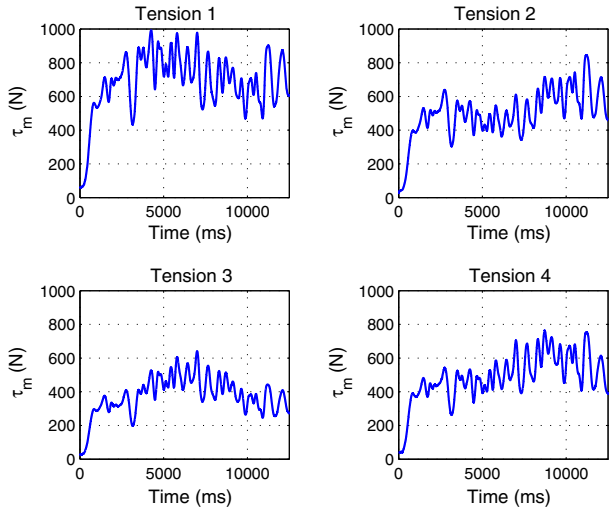

Fig. 9. Cables tension in the second experiment.

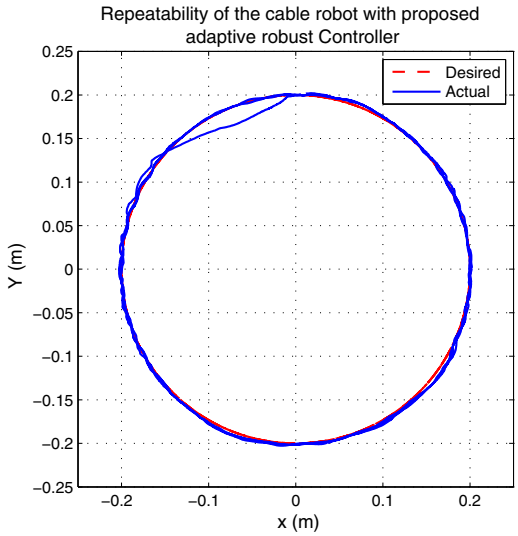

Fig. 10. Repeatability test of the cable robot using the proposed controller.

robust controller is much better than that of a well tuned PID controller or a pure sliding mode controller.

In order to compare the results quantitatively, the Euclidean and infinity norm of errors are given in Table 2. As it is seen in this table, the implementation results of the proposed adaptive robust controller (ARC) is significantly better than that of PID controller and sliding mode controller (SMC) in terms of all performance indices, and for both experiment sets. In this table, $L_2[e] = \sqrt{(1/T_f)\int_0^{T_f}|e|^2 dt}$ denotes normalized Euclidean norm for the entire error curve $e(t)$ in which T_f represents the total implementation time. Moreover, $L_\infty[e]$ denotes infinity norm of the error vector.

Repeatability criteria of a robot is most commonly used than absolute accuracy in industrial applications. For this reason, and in order to evaluate repeatability measure of the cable robot using the proposed controller, a final experiment is performed and reported in here. In this experiment, the desired circular trajectory with radius of 0.2 m is considered for three turns. Fig. 10 illustrates the repeatability performance of the proposed controller in this experiment. As it is seen in this figure, the proposed controller can compensate the small errors in the first turn, and track the circular trajectory in the remaining turns with very small errors and in order of 10^{-3}. Therefore, the proposed controller has a suitable absolute positioning accuracy with a better repeatability performance.

From the above experimental results, it may be concluded that the proposed adaptive robust controller can achieve suitable tracking performance for different desired trajectories, while it is more robust against structured and parametric uncertainties. Hence, it might be considered as a suitable solution for different cable robotic applications.

5. Conclusions

This paper addresses adaptive robust control of fully-constrained cable driven parallel robots. Since kinematic and dynamic models of the such robot are inevitably contaminated with unmodeled dynamics, parametric uncertainties and external disturbances, an adaptive robust sliding mode control is proposed to counteract these bounded uncertainties. The proposed controller does not require to generate any regression matrix of the kinematic and dynamic models of the robot. In addition, it keeps all cables under tension for the whole controllable workspace of the robot. It is proven that using such controller the tracking errors are uniformly ultimately bounded. Finally, the suitable tracking performance of the proposed controller is verified through some experiments on a planar cable driven parallel robot, and compared with two other controller schemes.

References

[1] Taghirad Hamid D, Nahon Meyer. Kinematic analysis of a macro–micro redundantly actuated parallel manipulator. Adv Rob 2008;22(6–7):657–87.
[2] Cone LL. Skycam: an aerial robotic camera system. Byte 1985;10(10):122–32.
[3] Kawamura Sadao, Kino Hitoshi, Won Choe. High-speed manipulation by using parallel wire-driven robots. Robotica 2000;18(01):13–21.
[4] Albus James, Bostelman Roger, Dagalakis Nicholas. The NIST robocrane. J Robot Syst 1993;10(5):709–24.
[5] Gouttefarde Marc, Gosselin Clément M. Analysis of the wrench-closure workspace of planar parallel cable-driven mechanisms. IEEE Trans Rob 2006;22(3):434–45.
[6] Wu Jun, Wang Jinsong, Wang Liping, Li Tiemin. Dynamics and control of a planar 3-DOF parallel manipulator with actuation redundancy. Mech Mach Theory 2009;44(4):835–49.

Table 2
Performance index for desired trajectories.

Performance indices		$L_2[e]$			$L_\infty[e]$		
Direction		x (mm)	y (mm)	ϕ (rad)	x (mm)	y (mm)	ϕ (rad)
Experiment set 1	PID	148	642	0.27	15	46	0.05
	SMC	54	518	0.34	7	62	0.08
	ARC	48	221	0.15	8	35	0.03
Experiment set 2	PID	692	735	0.42	58	76	0.07
	SMC	591	651	0.40	63	70	0.05
	ARC	335	436	0.23	45	41	0.02

[7] Wu Jun, Li Tiemin, Wang Jinsong, Wang Liping. Stiffness and natural frequency of a 3-DOF parallel manipulator with consideration of additional leg candidates. Robot Auton Syst 2013;61(8):868–75.
[8] Fang Shiqing, Franitza Daniel, Torlo Marc, Bekes Frank, Hiller Manfred. Motion control of a tendon-based parallel manipulator using optimal tension distribution. IEEE/ASME Trans Mechatron 2004;9(3):561–8.
[9] Reichert Christopher, Müller Katharina, Bruckmann Tobias. Robust internal force-based impedance control for cable-driven parallel robots. In: Cable-driven parallel robots. Springer; 2015. p. 131–43.
[10] Zi Bin, Duan BY, Du JL, Bao H. Dynamic modeling and active control of a cable-suspended parallel robot. Mechatronics 2008;18(1):1–12.
[11] Dewdney Peter, Nahon Meyer, Veidt Bruce. The large adaptive reflector: a giant radio telescope with an aero twist. Can Aeronaut Space J 2002;48(4):239–50.
[12] Duan BY, Qiu YY, Zhang FS, Zi B. On design and experiment of the feed cable-suspended structure for super antenna. Mechatronics 2009;19(4):503–9.
[13] Dallej Tej, Gouttefarde Marc, Andreff Nicolas, Dahmouche Redwan, Martinet Philippe. Vision-based modeling and control of large-dimension cable-driven parallel robots. In: 2012 IEEE/RSJ international conference on Intelligent Robots and Systems (IROS). IEEE; 2012. p. 1581–6.
[14] Chellal Ryad, Cuvillon Loïc, Laroche Edouard. A kinematic vision-based position control of a 6-DoF cable-driven parallel robot. In: Cable-driven parallel robots. Springer; 2015. p. 213–25.
[15] Khosravi Mohammad A, Taghirad Hamid D. Robust PID control of fully-constrained cable driven parallel robots. Mechatronics 2014;24(2):87–97.
[16] Oh So-Ryeok, Agrawal Sunil K. Generation of feasible set points and control of a cable robot. IEEE Trans Rob 2006;22(3):551–8.
[17] Khosravi Mohammad A, Taghirad Hamid D. Dynamic analysis and control of fully-constrained cable robots with elastic cables: variable stiffness formulation. In: Cable-driven parallel robots. Springer; 2015. p. 161–77.
[18] Oh So-Ryeok, Agrawal Sunil Kumar. Cable suspended planar robots with redundant cables: controllers with positive tensions. IEEE Trans Rob 2005;21(3):457–65.
[19] Williams Robert L, Gallina Paolo, Vadia Jigar. Planar translational cable-direct-driven robots. J Rob Syst 2003;20(3):107–20.
[20] Kino Hitoshi, Yahiro Toshiaki, Takemura Fumiaki, Morizono Tetsuya. Robust PD control using adaptive compensation for completely restrained parallel-wire driven robots: translational systems using the minimum number of wires under zero-gravity condition. IEEE Trans Rob 2007;23(4):803–12.
[21] Babaghasabha Reza, Khosravi Mohammad A, Taghirad Hamid D. Adaptive control of KNTU planar cable-driven parallel robot with uncertainties in dynamic and kinematic parameters. In: Cable-driven parallel robots. Springer; 2015. p. 145–59.
[22] El-Ghazaly Gamal, Gouttefarde Marc, Creuze Vincent. Adaptive terminal sliding mode control of a redundantly-actuated cable-driven parallel manipulator: CoGiRo. In: Cable-driven parallel robots. Springer; 2015. p. 179–200.
[23] Oh So-Ryeok, Albus James S, Mankala Kalyan, Agrawal Sunil K. A dual-stage planar cable robot: dynamic modeling and design of a robust controller with positive inputs. J Mech Des 2005;127:612.
[24] Behzadipour Saeed, Khajepour Amir. Stiffness of cable-based parallel manipulators with application to stability analysis. J Mech Des 2006;128:303.
[25] Opal-RT Company. RT-LAB version 8 User Guide; 2005.
[26] Babaghasabha Reza, Khosravi Mohammad A, Taghirad Hamid D, Vision based PID control on a planar cable robot. In: The 22nd iranian conference on electrical engineering. Tehran, Iran; 2014.
[27] Harris Chris, Stephens Mike. A combined corner and edge detector, in: Alvey vision conference, vol. 15. Manchester, UK; 1988. p. 50.
[28] Meunier Gabriel, Boulet Benoit, Nahon Meyer. Control of an overactuated cable-driven parallel mechanism for a radio telescope application. IEEE Trans Control Syst Technol 2009;17(5):1043–54.